Check for updates

Phosphorescent 2-phenylbenzothiazole Pt[IV] bis-cyclometalated complexes with phenanthroline-based ligands†

Andrea Corral-Zorzano, David Gómez de Segura, Elena Lalinde [ID] * and M. Teresa Moreno [ID] *

We describe a family of dicationic heteroleptic complexes of the type [Pt(pbt)₂(N^N)]Q₂, bearing two cyclometalating 2-phenylbenzothiazole (pbt) groups and a N^N phenanthroline-based ligand [N^N = 1,10-phenanthroline (phen) **4**, pyrazino[2,3-*f*][1,10]-phenanthroline (pyraphen) **5**, 5-amine-1,10-phenanthroline (NH₂-phen) **6**], with two different counteranions (Q = CF₃CO₂ and PF₆). Complexes **4–6-PF₆** and **4–6-CF₃CO₂** were obtained through ligand substitution from *cis*-[Pt(pbt)₂Cl₂] **2** and *cis*-[Pt(pbt)₂(OCOF₃)₂] **3**, respectively. The molecular structures of **2**, **3** and **4-PF₆** and the photophysical and electrochemical properties of all complexes were studied in detail. The precursors **2** and **3** exhibit high-energy emissions from ³IL excited states centered on the cyclometalated pbt, with lower efficiency in **2** in relation to **3** by the presence of closer thermally accessible deactivating ³LMCT excited states in **2**. The Pt[IV] complexes **4–5-CF₃CO₂/PF₆** display orange emission in CH₂Cl₂ solution, solid state (298, 77 K) or PS films, arising from a ³IL(pbt) emissive state. The NH₂-phen derivatives **6-CF₃CO₂/PF₆** show dual emission associated to two close different emissive states, ³IL′CT (L′ = NH₂-phen) and ³IL(pbt), depending on the medium and the excitation wavelength. DFT and time-dependent TD-DFT calculations support these assignments and allow explain the luminescence of these tris-chelate Pt[IV] complexes.

Introduction

Phosphorescent transition metal complexes have played a leading role in photochemical application, in particular in light-emitting materials,[1] chemosensing,[2] bioimaging,[2a,3] photodynamic therapy[4] and photocatalysis.[5] Among the transition metal complexes, cyclometalated Ir[III6] and Pt[II,b,c,6d,7] complexes have been deemed the most efficient because of their highly efficient populations of triplet excited states, which induce radiative decay processes and high tunability. In contrast, the excited-state properties of cyclometalated Pt[IV] complexes have started to be studied only recently. These complexes usually exhibit emitting excited states of ligand-centered (³LC) character with very low metal-to-ligand charge transfer (³MLCT) contribution. In general, the properties of the MLCT,

Departamento de Química-Centro de Síntesis Química de La Rioja (CISQ), Universidad de La Rioja, 26006 Logroño, Spain. E-mail: elena.lalinde@unirioja.es, teresa.moreno@unirioja.es

which determines the excited-states properties and the effectiveness of the spin–orbit coupling, depends on the coordination environment.[8] Although in most of the reported examples the Pt contribution is usually enough to facilitate the intersystem crossing (ISC) leading to phosphorescent complexes, in some of them with highly conjugate chromophores, there is a significant contribution of ligand fluorescence.[9] However, one of the major drawbacks to get efficient phosphorescent Pt[IV] emitters is the presence of thermally accessible ligand-to-metal charge transfer (LMCT) excited states, which usually provide nonradiative deactivation pathways.[8c,d,10] It has been demonstrated that the coordination of strong σ-donor ligands increases the energy of the LMCT states, thus leading to lower nonradiative rates and better emission efficiencies.[8c,e,10,11] To get efficient compounds, the presence of at least two cyclometalated ligand is required. Among them, several series of bis-cyclometalated Pt[IV] symmetrical or unsymmetrical with a variety of ligands in the two remaining *cis*-disposed coordination position have been reported.[8a,c–e,9a,10,11c,12] This category covers systems with both identical[8a,c,e,11c,12] or different[8d,9a,10,11b,13] cyclometalated groups and strong σ-donors as Me,[8c,11c] aryl,[8a,e,9a] dimetalated biaryl,[14] dithiolate,[15] aryl-NHC (C^C*)[10] ligands or derivatized cyclometalating ligands chosen to show liquid crystallinity behavior.[12] With

tridentate cyclometalated ligands, there are few reported examples. Among them, compounds of the form $[Pt(C^\wedge N^\wedge C)(C^\wedge C^*)Cl]$,[11b] $[Pt(N^\wedge N^\wedge C)(C^\wedge N)Cl]^+$ and the bis-tridentate $[Pt(N^\wedge N^\wedge C)_2]^{2+16}$ have been described. Respect to tris-cyclometalated Pt^{IV} compounds, several families of cationic homoleptic complexes mer/fac-$[Pt(C^\wedge N)_3]^+$ and heteroleptic $[Pt(C^\wedge N)_2(C^\wedge N')]^+$ have been described, being the fac-$[Pt(C^\wedge N)_3]^+$ the most efficient emitters.[8b,13,17] Related to these, dicationic tris-chelate compounds bearing one diimine chelating ligand of the type $[Pt(C^\wedge N)_2(N^\wedge N)]^{2+}$ are known, being $N^\wedge N'$ bipyridine-based ligands.[18] Similarly to other class of tris-chelate metal complexes, it is expected that replacing bpy by other α-diimines with more pronounced electron-withdrawing properties and/or low-lying excited states can result in notable changes in the luminescent properties within the $[Pt(C^\wedge N)_2(N^\wedge N)]^{2+}$ series. Among the potential $N^\wedge N$ ligands with these properties, 1,10-phenanthroline (phen) based ligands can be considered as the first choice by their available structural modifications.[19] Substitution and extension of the parent phen molecule would allow modifying its electron-acceptor character and affect the energy of its lowest triplet excitation state.

Here we present the synthesis, characterization, optical properties and theoretical calculations of heteroleptic Pt^{IV} complexes $[Pt(C^\wedge N)_2(N^\wedge N)]Q_2$ with two different kinds of counterions $[Q = CF_3CO_2$ (4–6-CF_3CO_2) and PF_6 (4–6-PF_6)] bearing 2-phenylbenzothiazol (pbt) as cyclometalated $C^\wedge N$ ligand and a phenanthroline-based $N^\wedge N$ ligand $[N^\wedge N$ = 1,10-phenanthroline (phen) 4, pyrazino[2,3-f][1,10]-phenanthroline (pyraphen) 5, 5-amine-1,10-phenanthroline (NH$_2$-phen) 6], aimed at the elucidation of the effect of the $N^\wedge N$ auxiliary ligands on their luminescence. The photophysical properties of these compounds and the corresponding starting materials, cis-$[Pt(pbt)_2(OCOF_3)_2]$ and cis-$[Pt(pbt)_2Cl_2]$, are described in detail in several media, and DFT and TD-DFT calculations are applied to support their absorption and emission spectra.

Results and discussion

Synthesis and characterization

The synthesis of the target dicationic bis(cyclometalated) Pt^{IV} complexes with phenanthroline-based ligands, $[Pt(pbt)_2(N^\wedge N)]^{2+}$, was achieved by using Pt^{II} and Pt^{IV} precursors that determine the $trans$-N,N arrangement of the pbt units (Scheme 1). Thus, for the preparation of the Pt^{IV} starting material cis-$[Pt(pbt)_2Cl_2]$ (2) we used as primary precursor the yellow Pt^{II} complex $[Pt(pbt)Cl(Hpbt-\kappa N)]$ (1), in which the pbt and Hpbt groups are in a N,N $trans$-configuration.[20] The oxidation reaction of this Pt^{II} derivative (1) with PhICl$_2$ at 0 °C produces the concomitant metalation of the pendant phenyl group of the Hpbt ligand (Scheme 1(i)). Previous reported studies of the oxidation of Pt^{II} cyclometalated derivatives with PhICl$_2$ proposed as the first step of the mechanism the electrophilic attack and the incorporation of a Cl$^+$, on the opposite face of the N-coordinated ligand, to generate the cationic pen-
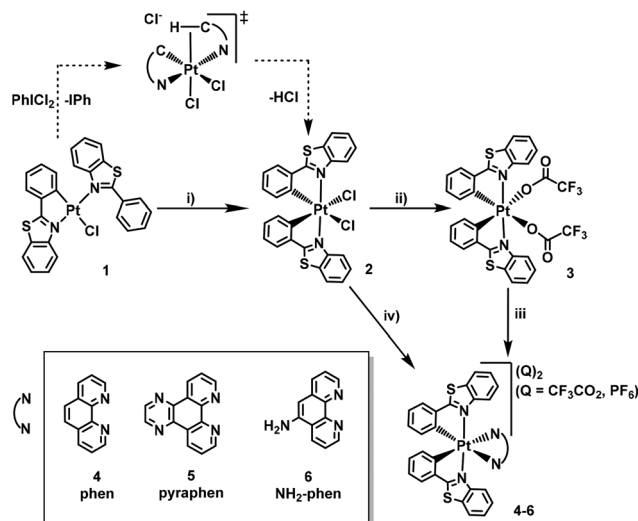
Scheme 1 Reagents and conditions: (i) PhICl$_2$ (1.3 equiv.), CH$_2$Cl$_2$, 0 °C; (ii) AgCF$_3$CO$_2$ (2.1 equiv.), acetone reflux 6 h; (iii) $N^\wedge N$ (1 equiv.); CH$_2$Cl$_2$ 3 h (for 4-CF_3CO_2 and 5-CF_3CO_2) or CH$_2$Cl$_2$/^{i}PrOH reflux 48 h (for 6-CF_3CO_2); (iv) $N^\wedge N$ (2 equiv.), TlPF$_6$ (4 equiv.) KClO$_4$ (30 equiv.); C$_2$H$_4$Cl$_2$ reflux 14 h (for 4-PF_6 and 6-PF_6) or 24 h (for 5-PF_6).

tacoordinate complex stabilized by the C–H agostic interaction of the pendant ligand. Finally, a fast proton transfer to a Cl$^-$ would produce HCl and the complex cis-$[Pt(pbt)_2Cl_2]$ (2) with $trans$-N,N; cis-C,C stereoselectivity.[9a] The generation of HCl makes necessary to bubble nitrogen meanwhile the reaction takes place to avoid the displacement of the cyclometalated ligand by the chloride atom.[11c]

Treatment of cis-$[Pt(pbt)_2Cl_2]$ 2 with two equiv. of silver trifluoroacetate in refluxing acetone produces the substitution of the Cl$^-$ ligands and the coordination of the CF$_3$COO$^-$ (κO), generating the neutral complex cis-$[Pt(pbt)_2(OCOCF_3)_2]$ (3) (Scheme 1(ii)). This compound is very useful as synthetic platform because of the lability of the trifluoroacetate groups, which would allow the substitution by a wide variety of ligands. Thus, the target dicationic phenanthroline-based bis-(cyclometalated) derivatives $[Pt(pbt)_2(N^\wedge N)](CF_3CO_2)_2$ (phen 4-CF_3CO_2, pyraphen 5-CF_3CO_2) were obtained by reacting 3 with the corresponding $N^\wedge N$ ligand under mild conditions. However, the synthesis of $[Pt(pbt)_2(NH_2$-phen)]$(CF_3CO_2)_2$ (6-CF_3CO_2) requires more drastic conditions (see Scheme 1(iii) and Experimental section). Crystallization of these complexes in several mixtures of solvents afforded always crystals of the starting material cis-$[Pt(pbt)_2(OCOCF_3)_2]$ (3). With the aim to obtain suitable crystals for X-ray diffraction analysis and also analyse the influence of the counteranion on the properties of the compounds, the related $[Pt(pbt)_2(N^\wedge N)]Q_2$ with Q = PF$_6$ as counteranion were synthesized. The reaction of cis-$[Pt(pbt)_2Cl_2]$ 2 with the corresponding $N^\wedge N$ ligand in the presence of TlPF$_6$ and KClO$_4$ (excess) refluxed in 1,2-dichloroethane (14–24 h) (see Scheme 1(iv) and Experimental section) allowed to obtain the related $[Pt(C^\wedge N)_2(N^\wedge N)](PF_6)_2$ (phen 4-PF_6, pyraphen 5-PF_6, NH$_2$-phen 6-PF_6) derivatives. These com-

pounds were isolated as pale-yellow (**2**, **3**), pale-orange (**4–5**)-CF_3CO_2, pale-pink (**4-PF_6**), white (**5-PF_6**) or orange (**6-CF_3CO_2/PF_6**) solids, consisting of racemic mixtures of Δ and Λ enantiomers with good yields and purities, according to analytical and spectroscopic data.

All derivatives were fully characterized by IR spectroscopy, matrix assisted laser desorption ionization time-of-flight (MALDI-TOF) mass spectrometry, 1D-NMR (^{1}H and ^{13}C{^{1}H}) and 2D-NMR experiments [^{1}H–^{1}H (COSY, TOCSY) and ^{1}H–^{13}C (HSQC, HMBC)] (see Experimental section and Fig. S1–S8†). The Pt^{IV} complexes **2** and **3** show in the MALDI-TOF mass spectra in a positive mode, the peak corresponding to the mass molecular with Na$^+$ ([M + Na]$^+$ m/z 709 **2**, 865 **3**) and those corresponding to the loss of one or two anionic co-ordinated groups (m/z 651 [M − Cl]$^+$ **2**; 728 [M − CF_3CO_2]$^+$, 616 [M − 2CF_3CO_2]$^+$ **3**). Complexes **4–6-CF_3CO_2** exhibit the corresponding [M − 2CF_3CO_2]$^+$ and [M − pbt − 2CF_3CO_2]$^+$ peaks, whereas complexes **4–6-PF_6** exhibit [M − 2PF_6]$^+$ as the parent peak, together with [M − N$^\wedge$N − 2PF_6]$^+$ or [M − pbt − 2PF_6]$^+$ (**4**, **6**). The IR spectra display characteristic vibrations corresponding to the Pt–N bond (442–487 cm^{-1}), ν(Pt–Cl) for **2** (332 cm^{-1}), ν(C=O) (1687–1699 cm^{-1} **3**, **4--6-CF_3CO_2**) and ν(PF_6) (~560, 840 cm^{-1} **4–6-PF_6**).

The C_2-symmetrical complexes (**2–5**) show in their ^{1}H and ^{13}C{^{1}H} NMR spectra one set of signals corresponding to the equivalent pbt ligands and to a half of the N,N'-donor ligand for **4–5-CF_3CO_2/PF_6**. However, the complexes **6-CF_3CO_2/PF_6**, with an unsymmetrical coordination environment around the Pt centre caused by the amine group on the phenanthroline ancillary ligand, display the expected two sets of signals corresponding to the non-equivalent cyclometalated groups. The most characteristic resonance in their ^{1}H NMR spectra is the proton in the *ortho* position to the C metalated of the pbt ligand (H^{11} and H$^{11'}$ for **6**), which appear as an upfield doublet with platinum satellites, with an important decrease of the $^3J_{Pt–H}$ (28.7–32.6 Hz) compared to the Pt^{II} complex **1** ($^3J_{Pt–H}$ 46.5 Hz), in coherence with the oxidation of the Pt^{II} to Pt^{IV}.[8a,17b] A clear difference between the complexes **4** and **5** with CF_3CO_2 and PF_6 counterions is the characteristic H^7 proton, which remains as a doublet at high frequency for **4,5-CF_3CO_2** (δ 9.35), as in the precursor **3** (δ 9.36), whereas for **4,5-PF_6** the H^7 proton suffers the expected strong upfield shift (δ 5.99 **4-PF_6**, 6.16 **5-PF_6**), due to the anisotropic shield of the aromatic phen-based ligand. Both complexes **6** locate the H^7 and H$^{7'}$ protons also at low frequency (δ 6.06, 5.97 **6-CF_3CO_2**, 6.09, 6.02 **6-PF_6**), but the NH$_2$ signal suffers a variation probably due to some interaction with the counteranion (δ 7.69 **6-CF_3CO_2**, 6.76 **6-PF_6**). The presence in the ^{19}F{^{1}H} NMR spectrum of **3** of one singlet at around −74.9 ppm with platinum satellites due to four-bond coupling ($^4J_{Pt–F}$ 4.6 Hz) confirms the coordination of the trifluoroacetate groups to the Pt^{IV} center. By contrast, only a singlet signal but without platinum satellites is observed for complexes **4–6-CF_3CO_2**. Complexes **4–6-PF_6** display the expected doublet (~−72.5 ppm, $^1J_{F–P}$ 709 Hz) and septuplet (~−145 ppm) in the ^{19}F{^{1}H} and ^{31}P{^{1}H} NMR spectra. The ^{13}C{^{1}H} NMR spectra of the complexes **3**, **4–6-**

CF_3CO_2/PF_6 show, as the most deshielded resonance, a singlet signal with ^{195}Pt satellites (75–91 Hz) corresponding to the C^2 (C^2 and C$^{2'}$ for **6**) of the pbt ligand. Furthermore, the signals for the CF_3CO_2$^−$ groups are visible for the complexes **3**, **4–5-CF_3CO_2** as two signals at 168.8 and 116.4 ppm, which appear resolved as quadruplets due to the coupling to the F atoms ($^2J_{C–F}$ 37 and $^1J_{C–F}$ 292 Hz, respectively).

X-Ray structures. The crystal structures of **2**, **3** and **4-PF_6** were solved by single crystals X-ray diffraction studies. The crystallographic data and selected bond lengths and angles are summarised in Table 1 and Tables S1, S2.† The molecules are chiral, although the complexes crystallize as a racemic in centrosymmetric groups (*Pbca* **2**, *P*2$_1$/*c* **3**, *Pbcn* **4-PF_6**) with the two enantiomers (Δ and Λ) in the unit cell. To simplify, only the Λ enantiomer of each structure is represented in Fig. 1. All Pt^{IV} complexes exhibit the expected distorted octahedral coordination with a symmetrical *trans*-N,N;*cis*-C,C disposition, which localizes the Cl$^−$ (**2**), OCOCF$_3$$^−$ (**3**) or both N donors of the phenanthroline ligand (**4-PF_6**) *trans* to the metalated carbons of the pbt ligands. The bite angles N–Pt–C of the pbt cyclometalated ligands are narrow [80.57(15)–81.31(18)°]. The angle between the two monodentate coligands (Cl$^−$ or $^−$OCOCF$_3$) is narrower in **3** [O(1)–Pt–O(3) 81.81(10)°] in relation to **2** [Cl(1)–Pt–Cl(2) 90.55(2)°], caused by the higher steric effect of the trifluoroacetate groups and, as expected, the angle for the N$^\wedge$N chelate is the smallest [78.9(2)°]. In complex

Table 1 Selected distances (Å) and angles (°) for **2**, **3** and **4-PF_6**

Parameter	2	3	4-PF_6
Pt–Cl/O/N_{N^N}	2.4439(6), 2.4418(6)	2.133(2), 2.158(3)	2.126(4)
Pt–N_{C^N}	2.0491(2), 2.0386(2)	2.031(2), 2.029(3)	2.055(4)
Pt–C	2.025(2), 2.022(2)	2.013(3), 2.031(4)	2.021(5)
N(1)–Pt–N(2)	170.62(8)	172.79(11)	169.4(2)
C–Pt–Cl/O/N_{N^N}	90.91(7), 87.94(6)	92.92(12), 98.25(12)	97.64(17)
C–Pt–N_{C^N}	81.14(9), 81.00(9)	81.83(12), 80.57(15)	81.31(18)
Cl/O/N_{N^N}–Pt–Cl/O/N_{N^N}	90.55(2)	81.81(10)	78.9(2)
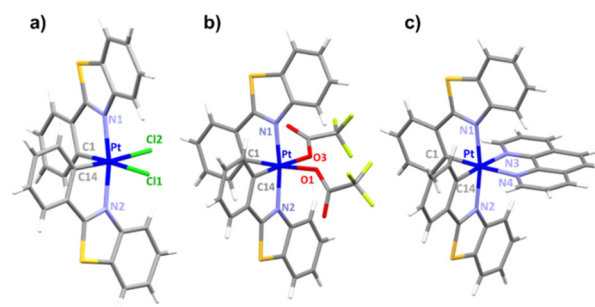
Fig. 1 Molecular structure of (a) **2**, (b) **3** and (c) the dication **4**$^{2+}$ in **4-PF_6**.

2, the Pt–Cl distances (~2.44 Å) are similar to those found for previously reported bis(cyclometalated) pentafluorophenyl complexes with Cl⁻ located *trans* position to the metalated carbon[8a,9a] and longer than those found in related compounds with Cl⁻ *trans* to the nitrogen of the cyclometalated unit (2.329 Å),[8d] in agreement with the higher *trans* influence of the C atom. In **3**, the Pt–O distances [*trans* to metalated carbon, 2.133(2), 2.158(3) Å] are similar to those found in the related complex with ppy, [Pt(ppy)₂(OCOCF₃)₂].[8c] In **4-PF₆**, the Pt–N distances of the N^N ligands [2.126(4) Å] are longer than that of the cyclometalated ligand [2.055(4) Å], thus demonstrating the high *trans* influence of the metalated carbon in the phenyl rings. The Pt–C distance is similar, within experimental error, to those in **2** and **3**. The torsion angles of the cyclometalated ligands (6.46°) and the N^N ligand (1.71°) are low, which impart a high degree of planarity on all ligands in **4-PF₆**.

In the supramolecular structure of **2**, weak intermolecular $\pi_{pbt}\cdots\pi_{pbt}$ interactions (minimum C–C distance 3.337 Å) and secondary Cl···H$_{pbt}$, Cl···S$_{pbt}$ and C$_{pbt}$···S$_{pbt}$ contacts can be observed. In **3**, the oxygens of the OCOCF₃ groups stablish intramolecular interactions with the π electron density of the benzothiazole group (2.817 Å) and *inter*molecular contacts with H or S of the pbt groups (Fig. S9 and S10†). The 3D-structure of **4-PF₆** is built up through the formation of some interactions involving the PF₆ anion and C–H secondary interactions of some rings (Fig. S11†).

Photophysical properties and theoretical calculations

Absorption properties and TD-DFT calculations. The UV-Vis absorption spectra of complexes **2**, **3**, **4–6-CF₃CO₂/PF₆**, collected in CH₂Cl₂ solution (5 × 10⁻⁵ M) at 298 K, are shown in Fig. 2 and the data summarized in Table S3.† Complex **1** shows a similar absorption pattern (Fig. S12†) than that previously reported for complex [Pt(pbt)(C₆F₅)(Hpbt-κN)].[21] Thus, the low-energy (LE) absorption band (425 nm) is assigned to a mixture of ¹IL (pbt) and ¹MLCT (Pt → pbt) transitions on the Pt(pbt) fragment. The UV-vis spectra of the Pt^IV derivatives display a similar intense absorption profile at high energies (λ < 280 nm), mainly ascribed to ¹IL (ππ*) transitions located on the aromatic ligands (pbt and N^N). The low energy absorption bands for **2**, **3**, **4–5-CF₃CO₂/PF₆** (~370 nm, ε = 25 400–11 500 M⁻¹ cm⁻¹) display similar pattern with slight variation in their maxima, whereas complexes **6** show, in

addition, two lowest-energy bands at ~400 nm (ε = 4850 M⁻¹ cm⁻¹) and 450–475 nm (ε ~ 1000 M⁻¹ cm⁻¹) red-shifted in relation to the precursor. To understand the nature of these experimental absorptions, TD-DFT/SCRF calculations in CH₂Cl₂ solution (PCM model) were done for **2**, **3** and the cations **4²⁺**–**6²⁺**. For **2** and **3**, the calculated bond distances and angles agree with those of the crystal structures, which ensure the accuracy of the DFT calculations at this level (Table S4†) and the calculated and the experimental spectra compare well (Fig. S13†). The largest deviation was found in the Pt–N bonds, which are larger by *ca.* 0.04 Å than those found in the molecular structures. Calculations for **2** and **3** indicate that the lowest excited state, with a great oscillator strength value (S₂ 350 nm **2**, S₁ 352 nm **3**), is contributed by a HOMO to LUMO transition (87% **2**, 92% **3**) (Tables S5, S6,† Fig. 3 and S14†). Both, the HOMO and the LUMO are distributed between both pbt ligands. Thus, the low-energy absorption can be attributed to an intraligand charge transfer ¹ILCT transition within the pbt ligands. In these complexes, the LUMO+2 has a notable contribution of Pt (41% **2**; 44% **3**) and is involved in close transitions (S₁, S₃ for **2** and S₂ for **3**), with low oscillator strength, that have a mixed ¹IL/¹LMCT character. For the dicationic compounds with phen (**4²⁺**) and pyraphen (**5²⁺**) ligands, the most intense calculated excitation is S₅ having mixed configuration in **4²⁺** (¹ILCT/¹LLCT/¹LL'CT calcd 348.6 nm) and ¹ILCT in **5²⁺** (calcd 349.5). In these complexes, the composition of the HOMO (and also H−1 and H−2) is very similar to that of **2** and **3**, but the LUMO is mainly located on the N^N ancillary ligands (94% **4²⁺**, 97% **5²⁺**). The close target orbitals L+1 and L+2 are composed from the pbt and, to a lesser extent, from the N^N and Pt, while L+3 has a notable metal contribution (36%). These orbitals are involved in the lowest S$_{1-4}$ transitions with mixed (¹ILCT/¹LLCT/¹LL'CT/¹LMCT S$_{1,2}$ **4²⁺**; S$_{1,3-4}$ **5²⁺**) or ¹LL'CT (S$_{3,4}$ **4²⁺**; S₂ **5²⁺**) contribution, but with negligible intensity (Table S5†). Finally, for the cationic **6²⁺** the lowest S₁ state (444 nm) is contributed by a HOMO to LUMO transition (87%) and HOMO to LUMO+1 (11%), being attributed to a ¹IL′CT from the amino group to the pyridinic ring of the phenanthroline ligand with minor contribution of ligand′-to-ligand charge transfer ¹L′LCT (NH₂-phen → pbt) transition.

Emission properties and theoretical calculations. Emissive properties of all complexes have been evaluated in degassed
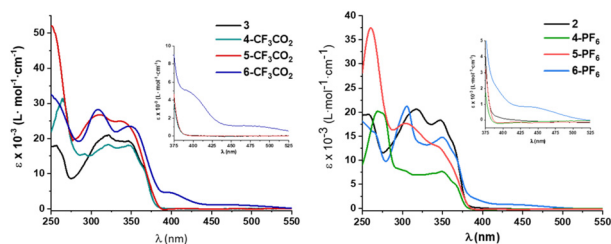
Fig. 2 UV-Vis absorption spectra of complexes **4–6-CF₃CO₂**, **4–6-PF₆** and the corresponding precursors, **3** and **2**, respectively.
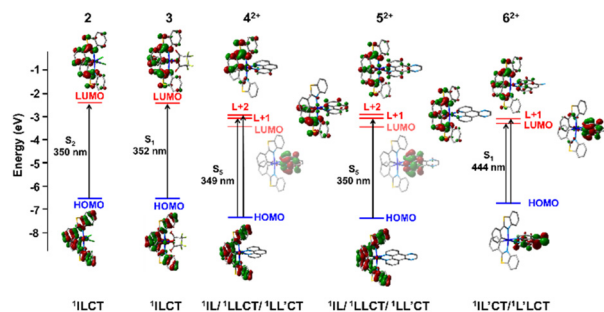

Fig. 3 Schematic representation of frontier orbitals and selected excitations for **2**, **3** and **4²⁺–6²⁺**. Transitions with the highest *f* oscillator strength in the LE region.

Table 2 Photophysical data for complexes **1**, **2**, **4–6-CF₃CO₂** and **4–6-PF₆** [a]

	CH₂Cl₂				PS 10 wt%			Solid	
	298 K			77 K	298 K			298 K	77 K
	λ_{max}[b]/nm	τ/µs	ϕ_{PL}	λ_{max}[b]/nm	λ_{max}[b]/nm	τ/µs	ϕ_{PL}	λ_{max}[b]/nm	λ_{max}[b]/nm
1	537	8.7	0.09	530	537	9.1	0.17	550	550
2	511	11.4	<0.01	506	555	15.5	0.02	644	529
3	511	10.8	0.02	501	547	14.0	0.11	539	521
4-CF₃CO₂	513	10.3	0.02	501	513	22.4	0.03	505	517
4-PF₆	[c]	—	—	534	556	12.3	0.01	609	516
5-CF₃CO₂	511	10.4	0.01	501	515	21.1	0.03	501	529
5-PF₆	[c]	—	—	538	530	11.4	0.01	590	520
6-CF₃CO₂	[c]	—	—	503[a], 630[d]	514	22.8	0.02	662[e]	667
6-PF₆	565	11.5	<0.01	610[e]	582[f]	15.4	<0.01	638[e]	644

[a] λ_{ex} 365 nm. [b] Highest energy peaks of the phosphorescent band. [c] Non-emissive. [d] λ_{ex} 395 nm. [e] λ_{ex} 440 nm. [f] PS 5%.

CH₂Cl₂ solutions (5 × 10⁻⁵ M), solid state (298 and 77 K) and polystyrene films (PS, 10 wt%). Photophysical data are summarized in Table 2. The Pt[II] precursor **1** displays in all media a typical vibronically structured band at ∼540 nm assigned, according to related derivatives,[9a,21] to a mixture of ³IL/³MLCT centered on the Pt(pbt) fragment (Fig. S15†). These characteristics, together with the lifetimes in the microseconds range (τ = 9.1 µs PS; 8.7 µs, CH₂Cl₂ 298 K), are characteristic of a phosphorescent emission. Interestingly, the quantum yield reaches the 17% in doped PS film.

The Pt[IV] complexes are emissive with lifetimes in the range of microseconds (µs) regime. To confirm the nature of the emissions, the lowest TD-DFT (T₁–T₃) vertical triplet excitations at the S₀ geometry (Table S5†) and the corresponding optimized lowest-energy triplet excited states (T₁–T₃) were calculated and detailed in Table S8.† The energy values of each state and geometries are depicted in the ESI (Table S9 and *xyz* files†). The Pt[IV] precursors **2** and **3**, featuring Cl⁻ or OCOCF₃⁻ ligands respectively, show vibronically structured bands in solution (λ_{max} 511 nm) and glasses, red shifted in PS films (∼550 nm Fig. 4a and Table 2). For both complexes, the two lowest-energy vertical triplet excitations T₁,₂ at the S₀ geometry

are calculated at *ca.* 469 nm and have ³IL nature located on the pbt. The optimized T₁ states (see SOMO and SOMO−1, Table S7†) and the spin density surfaces indicate also ³IL emission character centered on one pbt ligand (Fig. 4). The lifetimes for both complexes are very similar in CH₂Cl₂ solution and in PS at room temperature (10.8–15.5 µs) and slightly higher than in the Pt[II] derivative **1** (see Table 2), according to a lower ³MLCT contribution in the excited state.

The quantum yields of both complexes are comparable in solution (ϕ < 1% **2** and 2% **3**), but in PS the complex **3** displays an efficiency 10-fold than **2** (ϕ 2% **2** *vs.* 11% **3**). This behaviour could be explained analysing the character of the T₃ vertical excitation. In complex **3**, the following S₀ → T₃ excitation shows a ³IL nature and it is 0.64 eV above T₁/T₂, whereas in **2**, T₃ exhibits a ³LMCT character and is closer to T₁/T₂ (0.57 eV). This could favour the promotion of the excited molecules of complex **2** to this non-radiative state, producing a detriment on the emission efficiency (Fig. 4b).

Dicationic complexes **4-PF₆** and **5-PF₆** are not emissive in CH₂Cl₂ solution at room temperature, caused surely by a vibrational overlap between close energy triplet excited states and the ground state, favouring a radiationless deactivation. However, complexes **4-CF₃CO₂** and **5-CF₃CO₂** display typical weak structured bands that become more intense at 77 K and in PS films (Fig. 5). The PF₆ complexes (**4-PF₆** and **5-PF₆**)
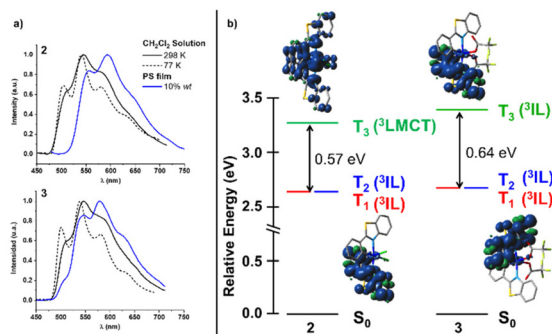
Fig. 4 (a) Emission spectra (λ_{exc} 365 nm) of **2** and **3** in CH₂Cl₂ solution (298 and 77 K) and PS film (10 wt%) and (b) spin density distribution and relative energies of the vertical triplet excitations (T₁–T₃) at the ground-state geometry for **2** and **3**.
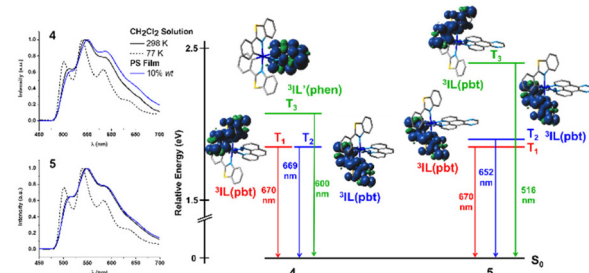
Fig. 5 Emission spectra in several media of **4-CF₃CO₂** and **5-CF₃CO₂** and the spin density distribution of the optimized T₁–T₃ excited states (λ_{em} calculated as the difference between the energies of the optimized triplet states and the singlet state at the triplet geometry).

exhibit similar patterns in glasses and PS films, but slightly red-shifted in relation to those of CF_3CO_2 (*i.e.*, λ_{max} 556 nm **4-PF$_6$** *vs.* 513 nm **4-CF$_3$CO$_2$**, PS films) (Fig. S16†). According to calculations for the dications **4^{2+}** and **5^{2+}**, the SOMO and SOMO−1 and the spin density surface in the T$_1$ optimized state are located on one pbt ligand, suggesting a ^{3}IL character of the emission band. The excited triplet states T$_1$/T$_2$, both centered on one pbt, are very close in energy. The T$_3$ state (centered in the phen ligand in **4^{2+}**) could be indicative of a mixture of ^{3}IL/^{3}IL′ (L′ = N^N), whereas in **5^{2+}** the T$_3$ state of nature ^{3}IL (pbt) is far of T$_2$/T$_1$ and thus, the emission is assigned to a ^{3}IL state with no contribution of the pyraphen ligand (Fig. 5).

The NH$_2$-phen derivative **6-CF$_3$CO$_2$** is non-emissive in solution at room temperature, but it displays a structured emission in PS film (514 nm) and two different emission bands, that can be selected by the excitation wavelength, in glassy solution (Fig. 6). One of them has the typical structured pattern at 503 nm, similar to those found for previously mentioned complexes, and other broader and red shifted band at ~630 nm, which can be selectively obtained upon excitation at λ_{exc} > 400 nm. Complex **6-PF$_6$** exhibits in CH_2Cl_2 solution and PS film a broad band at 565 and 582 nm, respectively, which is red-shifted in glasses (610 nm, Fig. 6). The lifetimes in PS films are, in average, larger in the CF_3CO_2 complexes than in the corresponding PF$_6$ (*i.e.* τ_{PS} 22.8 µs **6-CF$_3$CO$_2$** *vs.* 15.4 µs **6-PF$_6$**). For this complex, the lowest energy triplet vertical excitation T$_1$ (531 nm) with S$_0$ geometry has admixture of transitions from the NH$_2$ group to the aryl groups of the phenanthroline (^{3}IL′CT) with some of ^{3}L′LCT/^{3}L′MCT contribution. The S$_0$ → T$_2$ excitation (514 nm) has major ^{3}IL′CT character, whereas the T$_3$ is somewhat more complex (471 nm, ^{3}ILCT/^{3}LLCT/^{3}LMCT). The spin density surface of the optimized T$_1$ and T$_2$ states (738 and 739 nm) (Fig. 6) are mainly contributed from the NH$_2$-phen ligand and are assigned to the broad symmetrical band centered at 630 nm. The optimized T$_3$ excited state shows a ^{3}IL(pbt) character and can be associated to the structured band observed in glassy solution (~500 nm) (Fig. 6). The quantum yields in

CH_2Cl_2 solution or PS films of these Pt^{IV} complexes are relatively low (ϕ range < 1–3%).

In the solid state at room temperature all compounds show broader and asymmetrical bands, particularly red-shifted in **2**, **4–5-PF$_6$** (298 K) and **6-CF$_3$CO$_2$/PF$_6$** (298, 77 K, Fig. S17†). This phenomenon can be explained by the heterogeneity of the solids obtained by rapid precipitation and/or by the proximity of the different excited triplet states and the more difficult intersystem crossing caused by the rigidity of the media. In **2**, **4–5-PF$_6$**, the profiles become more structured at 77 K, indicating that the increased rigidity at low temperature decreases the electronic mixing of states.

Electrochemical properties

Cyclic voltammetry (CV) measurements in anhydrous CH_2Cl_2 for the Pt^{IV} complexes **2**, **3**, **4–6-CF$_3$CO$_2$** showed comparable redox behavior (Table 3). No oxidation waves were observed in the electrochemical window of the solvent. In the cathodic region, an irreversible reduction wave can be observed for all compounds in the range −1.61 to −1.63 *versus* Ag/AgCl, that remained irreversible at 100, 50 or 200 mV s^{-1} (Fig. S18† for 100 mV s^{-1}). For complex **6-CF$_3$CO$_2$**, this irreversible wave is positively shifted appearing at −1.56 V and it is accompanied of a quasi-reversible wave at −0.58 V, surely related with the reduction of the NH$_2$-phen amine ligand. Considering the null effect of the phenanthroline ligand in the irreversible reduction in complexes **4-CF$_3$CO$_2$** and **5-CF$_3$CO$_2$** and following the interpretation given by Bernhard *et al.*[18] for related dicationic $[Pt(C^N)_2(bpy)]^{2+}$ complexes, the electrochemical reduction is tentatively related to the reduction of the metal center with concomitant loss of the phenanthroline based ligand ($[Pt^{IV}(pbt)_2(N^N)]^{2+} \rightarrow [Pt^{II}(pbt)_2] + N^N$). Similar metal center reduction processes could also be associated to the irreversible reduction of the neutral derivatives **2** and **3**.

The reduction potentials should allow obtaining information about the LUMO. The LUMO energy levels were estimated from the CV data by using the following equation: $E_{LUMO} = -(E_{onset} + 5.1 - 0.45$ eV$)$, where 0.45 eV is the potential of the ferrocene *vs.* Ag/AgCl and 5.1 eV the energy level of ferro-
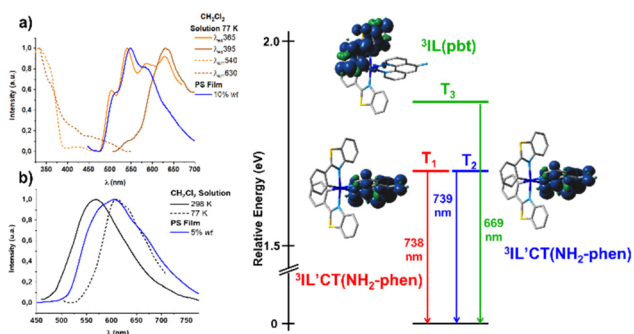
Fig. 6 Left: Emission spectra of (a) **6-CF$_3$CO$_2$** and (b) **6-PF$_6$** in several media. Right: Spin density distribution of the optimized T$_1$–T$_3$ excited states for **6^{2+}** (λ_{em} calculated as the difference between the energies of the optimized triplet states and the singlet state at the triplet geometry).

Table 3 Electrochemical data[a] and LUMO energy estimations for Pt^{IV} complexes

	2	**3**	**4-CF$_3$CO$_2$**	**5-CF$_3$CO$_2$**	**6-CF$_3$CO$_2$**
$E_p^{red\ b}$ (V)	−1.62	−1.61	−1.63	−1.63	−1.56 −0.58[c]
$E_{onset,red}$ (V)	−1.50	−1.49	−1.46	−1.50	−1.37 −0.45
E_{LUMO}^d (eV)	−3.15	−3.17	−3.18	−3.15	−3.27
E_{LUMO}^e (eV)	−2.41	−2.43	−3.31	−3.40	−3.24

[a] All measurements were carried out at 298 K in a 0.1 M solution of (NBu$_4$)PF$_6$ in dry CH_2Cl_2 at 100 mV s^{-1} *vs.* Ag/AgCl reference electrode. [b] Irreversible cathodic peak potentials. [c] $E_{1/2}$ for the quasi-reversible wave in **6-CF$_3$CO$_2$**. [d] Estimated LUMO energy by electrochemistry data $[E_{LUMO} = -(E_{onset,red} + 5.1 - E_{Fc/Fc^+})]$. [e] Estimated LUMO energy by DFT calculations.

cene to the vacuum energy level (Table 3). The calculated LUMO energies for **2**, **3**, **4–5-CF$_3$CO$_2$** are almost identical (−3.15 to −3.18 eV), what is in accordance with a LUMO (or target orbital) mainly located on the dicationic fragment "Pt(pbt)$_2^{2+}$". For **6-CF$_3$CO$_2$** the calculated energy is somewhat lower (−3.27 eV), which suggests some additional contribution of the NH$_2$-phen ligand to the LUMO, as it is supported by DFT calculations. As shown in Table 3, which includes the estimated LUMO energies (by CV and DFT calculations), only for complex **6-CF$_3$CO$_2$** the electrochemical LUMO energy fits reasonably well with that estimated by DFT calculations.

Conclusions

A series of phosphorescent bis-cyclometalated Pt^{IV} complexes with the pbt ligand, comprising [Pt(pbt)$_2$Cl$_2$] **2**, [Pt(pbt)$_2$(OCOF$_3$)$_2$] **3** and [Pt(pbt)$_2$(N^N)]Q$_2$ **4–6-CF$_3$CO$_2$/PF$_6$**, where N^N is a phenanthroline-based ligand and Q = CF$_3$CO$_2$ or PF$_6$, have been synthesized. Their photophysical properties have been analyzed with the support of DFT and TD-DFT calculations. The lowest absorption bands in the UV-vis absorption spectra are assigned to intraligand ^{1}ILCT (L = pbt) for **2** and **3** and ^{1}ILCT/^{1}LLCT/^{1}LL'CT (L' = phen) for **4–5-CF$_3$CO$_2$/PF$_6$**. The complexes **6-CF$_3$CO$_2$/PF$_6$** additionally exhibit a low energy band at ~450 nm, associated to a ^{1}IL'CT transition from the amine group to the pyridine ring of the phen ligand with minor contribution of ^{1}L'LCT (NH$_2$-phen → pbt) transition. The Pt^{IV} precursors **2** and **3** display phosphorescence from predominantly ^{3}IL(pbt) states. The lower efficiency in PS films of **2** in comparison to **3** can be explained by the assumption that a deactivating ^{3}LMCT excited state is lower in energy in **2**, becoming thermally accessible from the emitting state. The dicationic complexes **4–5-CF$_3$CO$_2$/PF$_6$** exhibit also weak emissions, which arise from essentially ^{3}IL(pbt) states. The NH$_2$-phen derivatives **6-CF$_3$CO$_2$/PF$_6$** exhibit dual phosphorescence at ~630 and 500 nm, as a consequence of the existence of two close ^{3}IL'CT(phen) and ^{3}IL(pbt) emissive states, respectively. The low quantum yields of these tris-chelate complexes indicates that the strategy of coordinating a rigid phenanthroline ligand has not been successful to increase the efficiency.

Conflicts of interest

There are no conflicts to declare.

Acknowledgements

References

1 (*a*) W. C. H. Choy, W. K. Chan and Y. Yuan, *Adv. Mater.*, 2014, **26**, 5368–5399; (*b*) T. Fleetham, G. Li and J. Li, *Adv. Mater.*, 2017, **29**, 1601861; (*c*) C. Cebrián and M. Mauro, *Beilstein J. Org. Chem.*, 2018, **14**, 1459–1481; (*d*) Y. Chi and P. T. Chou, *Chem. Soc. Rev.*, 2010, **39**, 638–655; (*e*) H. Xu, R. Chen, Q. Sun, W. Lai, Q. Su, W. Huang and X. Liu, *Chem. Soc. Rev.*, 2014, **43**, 3259–3302; (*f*) J. A. G. Williams, S. Develay, D. L. Rochester and L. Murphy, *Coord. Chem. Rev.*, 2008, **252**, 2596–2611; (*g*) L. Xiao, Z. Chen, B. Qu, J. Luo, S. Kong, Q. Gong and J. Kido, *Adv. Mater.*, 2011, **23**, 926–952.

2 (*a*) S. Abbas, I.-u.-D. Din, A. Raheel and A. Tameez ud Din, *Appl. Organomet. Chem.*, 2020, **34**, e5413; (*b*) D.-L. Ma, V. P.-Y. Ma, D. S.-H. Chan, K.-H. Leung, H.-Z. He and C.-H. Leung, *Coord. Chem. Rev.*, 2012, **256**, 3087–3113; (*c*) O. S. Wenger, *Chem. Rev.*, 2013, **113**, 3686–3733; (*d*) I. Omae, *J. Organomet. Chem.*, 2016, **823**, 50–75.

3 (*a*) K. Y. Zhang, Q. Yu, H. Wei, S. Liu, Q. Zhao and W. Huang, *Chem. Rev.*, 2018, **118**, 1770–1839; (*b*) M. Mauro, A. Aliprandi, D. Septiadi, N. S. Kehr and L. De Cola, *Chem. Soc. Rev.*, 2014, **43**, 4144–4166; (*c*) E. Baggaley, J. A. Weinstein and J. A. G. Williams, *Coord. Chem. Rev.*, 2012, **256**, 1762–1785.

4 (*a*) S. Monro, K. L. Colón, H. Yin, J. Roque, P. Konda, S. Gujar, R. P. Thummel, L. Lilge, C. G. Cameron and S. A. McFarland, *Chem. Rev.*, 2019, **119**, 797–828; (*b*) A. Zamora, G. Vigueras, V. Rodríguez, M. D. Santana and J. Ruiz, *Coord. Chem. Rev.*, 2018, **360**, 34–76; (*c*) L. K. McKenzie, H. E. Bryant and J. A. Weinstein, *Coord. Chem. Rev.*, 2019, **379**, 2–29; (*d*) J. Liu, C. Zhang, T. W. Rees, L. Ke, L. Ji and H. Chao, *Coord. Chem. Rev.*, 2018, **363**, 17–28; (*e*) C.-P. Tan, Y.-M. Zhong, L.-N. Ji and Z.-W. Mao, *Chem. Sci.*, 2021, **12**, 2357–2367.

5 (*a*) D. M. Arias-Rotondo and J. K. McCusker, *Chem. Soc. Rev.*, 2016, **45**, 5803–5820; (*b*) Y. You and W. Nam, *Chem. Soc. Rev.*, 2012, **41**, 7061–7084; (*c*) C. K. Prier, D. A. Rankic and D. W. C. MacMillan, *Chem. Rev.*, 2013, **113**, 5322–5363.

6 (*a*) J. C. Deaton and F. N. Castellano, in *Iridium(III) in Optoelectronic and Photonics Applications*, ed. E. Zysman-Colman, 2017, pp. 1–69. DOI: 10.1002/9781119007166.ch1; (*b*) F. Monti, A. Baschieri, L. Sambri and N. Armaroli, *Acc. Chem. Res.*, 2021, **54**, 1492–1505; (*c*) S. Lee and W.-S. Han, *Inorg. Chem. Front.*, 2020, **7**, 2396–2422; (*d*) Z. Feng, Y. Sun, X. Yang and G. Zhou, *Chem. Rec.*, 2019, **19**, 1710–1728; (*e*) R. Bai, X. Meng, X. Wang and L. He, *Adv. Funct. Mater.*, 2020, **30**, 1907169; (*f*) T.-Y. Li, J. Wu, Z.-G. Wu, Y.-X. Zheng, J.-L. Zuo and Y. Pan, *Coord. Chem. Rev.*, 2018, **374**, 55–92; (*g*) I. N. Mills, J. A. Porras and S. Bernhard, *Acc. Chem. Res.*, 2018, **51**, 352–364; (*h*) S. Yoon and T. S. Teets, *Chem. Commun.*, 2021, **57**, 1975–1988.

7 (*a*) J. Herberger and R. F. Winter, *Coord. Chem. Rev.*, 2019, **400**, 213048; (*b*) A. Haque, H. El Moll, K. M. Alenezi, M. S. Khan and W.-Y. Wong, *Materials*, 2021, **14**, 4236; (*c*) S. Huo, J. Carroll and D. A. K. Vezzu, *Asian J. Org. Chem.*,

2015, **4**, 1210–1245; (*d*) X. Wang and S. Wang, *Chem. Rec.*, 2019, **19**, 1693–1709; (*e*) T. Strassner, *Acc. Chem. Res.*, 2016, **49**, 2680–2689.

8 (*a*) N. Giménez, R. Lara, M. T. Moreno and E. Lalinde, *Chem. – Eur. J.*, 2017, **23**, 5758–5771; (*b*) F. Juliá and P. González-Herrero, *Dalton Trans.*, 2016, **45**, 10599–10608; (*c*) F. Juliá, M.-D. García-Legaz, D. Bautista and P. González-Herrero, *Inorg. Chem.*, 2016, **55**, 7647–7660; (*d*) Á. Vivancos, D. Poveda, A. Muñoz, J. Moreno, D. Bautista and P. González-Herrero, *Dalton Trans.*, 2019, **48**, 14367–14382; (*e*) J.-C. López-López, D. Bautista and P. González-Herrero, *Dalton Trans.*, 2021, **50**, 13294–13305.

9 (*a*) N. Giménez, E. Lalinde, R. Lara and M. T. Moreno, *Chem. – Eur. J.*, 2019, **25**, 5514–5526; (*b*) J. E. Expósito, M. Álvarez-Paino, G. Aullón, J. A. Miguel and P. Espinet, *Dalton Trans.*, 2015, **44**, 16164–16176.

10 Á. Vivancos, A. Jiménez-García, D. Bautista and P. González-Herrero, *Inorg. Chem.*, 2021, **60**, 7900–7913.

11 (*a*) Á. Vivancos, D. Bautista and P. González-Herrero, *Inorg. Chem.*, 2022, **61**, 12033–12042; (*b*) Á. Vivancos, D. Bautista and P. González-Herrero, *Chem. – Eur. J.*, 2019, **25**, 6014–6025; (*c*) F. Juliá, D. Bautista and P. González-Herrero, *Chem. Commun.*, 2016, **52**, 1657–1660.

12 R. R. Parker, J. P. Sarju, A. C. Whitwood, J. A. G. Williams, J. M. Lynam and D. W. Bruce, *Chem. – Eur. J.*, 2018, **24**, 19010–19023.

13 J. C. López-López, D. Bautista and P. González-Herrero, *Chem. – Eur. J.*, 2020, **26**, 11307–11315.

14 J.-C. López-López, D. Bautista and P. González-Herrero, *Chem. Commun.*, 2022, **58**, 4532–4535.

15 A. Ionescu, N. Godbert, I. Aiello, L. Ricciardi, M. La Deda, A. Crispini, E. Sicilia and M. Ghedini, *Dalton Trans.*, 2018, **47**, 11645–11657.

16 Y. M. Dikova, D. S. Yufit and J. A. G. Williams, *Inorg. Chem.*, 2023, **62**, 1306–1322.

17 (*a*) F. Juliá, D. Bautista, J. M. Fernández-Hernández and P. González-Herrero, *Chem. Sci.*, 2014, **5**, 1875–1880; (*b*) F. Juliá, G. Aullón, D. Bautista and P. González-Herrero, *Chem. – Eur. J.*, 2014, **20**, 17346–17359.

18 D. M. Jenkins and S. Bernhard, *Inorg. Chem.*, 2010, **49**, 11297–11308.

19 G. Accorsi, A. Listorti, K. Yoosaf and N. Armaroli, *Chem. Soc. Rev.*, 2009, **38**, 1690–1700.

20 Y. Zhou, J. Jia, L. Cai and Y. Huang, *Dalton Trans.*, 2018, **47**, 693–699.

21 J. R. Berenguer, J. G. Pichel, N. Giménez, E. Lalinde, M. T. Moreno and S. Piñeiro-Hermida, *Dalton Trans.*, 2015, **44**, 18839–18855.